An Active-Perturbation Method to Estimate Online Inertia and Damping in Electric Power Systems

Federico Bizzarri*, Angelo Brambilla*, Davide del Giudice* and Daniele Linaro*
*Politecnico di Milano, Department of Electronics, Information and Bioengineering
p.zza Leonardo da Vinci, 32, 20133 Milano, Italy
Email: {name.surname}@polimi.it

***Abstract*—An adequate level of power system inertia and load damping is essential to ensure frequency stability following power imbalances. Prior to that, however, it is first necessary to be capable of estimating these parameters. In this paper, we propose an original method to estimate the global inertia and damping of a power system comprising conventional synchronous generators, as well as modern generation units based on grid forming and following converters, which can provide virtual inertia and load damping. The effectiveness of our approach is tested on a modified version of the IEEE39 power system with ambient noise.**

***Index Terms*—inertia estimation, damping estimation, online estimation, active perturbation method, probing signal**

I. Introduction

Electric power systems are undergoing radical changes due to the increasing decarbonization in the energy production sector and the transition from massive generation units to smaller ones, scattered in the grid and used for self-consumption.

A noteworthy effect of this transition is the growing rate of converter-interfaced elements. This pertains not only to the generation side, where conventional synchronous generators (SGs) are being progressively replaced by converter-interfaced plants fueled by renewable energy sources (RES), but also to the consumption side. Indeed, conventional loads such as motors are connected more frequently to the grid through electrical drives.

Converter-interfaced generators and loads have different electrical characteristics from their conventional counterparts. A major difference is that the former do not naturally display inertia and (load) damping, unless converters are controlled to this specific aim. Thus, the phase-out of SGs, combined with the growing share of converter-interfaced elements, leads to a progressive degradation of system inertia and (load) damping.

Since both inertia and damping are of paramount importance in supporting frequency stability [1], the availability of reliable methods to estimate their actual amount becomes crucial to assessing whether actions ought to be taken in order to counteract frequency oscillations. These methods should be capable of estimating the *synthetic* inertia and damping implemented also at *control level* through grid-forming (GFM) and grid-following (GFL) converter-interfaced generators (CIGs). Synthetic inertia and damping contribute to the so-called fast frequency response (FFR), i.e., the ability of some resources, including converter-based generators and loads, to change the net power exchange much faster than conventional SGs through primary frequency response. We refer the interested reader to [2]–[4] and references therein for in-depth reviews of the inertia and damping estimation methods available in the literature.

Here we present a novel, reliable, and efficient method for the online estimation of *global inertia* and *global damping* of a power system. Our method belongs to the class of algorithms based on *active perturbations*, i.e., those characterized by probing signals [5] used for system identification purposes [6], [7]. The main source of inspiration for our work is in the realm of frequency synchronization of power generators [8], which is a necessary condition for the operation of electric power systems. During steady-state operation, the frequency is the same throughout the entire grid and each pair of generators has a fixed phase difference that determines the power flow. Although the focus of our work is not on synchronization but on estimating global inertia and damping, the main results we propose are grounded in this concept.

II. The power system model

A. The large-signal model

To introduce our results, it is useful to discuss what happens in a power system modeled in the dq-frame including N synchronous generators equipped with primary frequency control and whose dynamic evolution is modeled by the simple swing equation[1]. Generators are interconnected by lines and transformers, and constant-power and/or constant-impedance loads are connected to the grid buses. Under these assumptions, N subsets of related differential algebraic equations (DAEs) are introduced, one for each SG:

$$\begin{aligned} \dot{\delta}_j &= \Omega\left(\omega_j - \omega_0\right) \\ \mathcal{M}_j\dot{\omega}_j &= P_{m_j}(\boldsymbol{x}_j, \omega_j - \omega_0, \boldsymbol{y}_j) + \\ &\quad -P_{e_j}(\delta_1, \ldots, \delta_N) - \mathcal{D}_j(\omega_j - \omega_0) \\ \dot{\boldsymbol{x}}_j &= \boldsymbol{f}_j(\boldsymbol{x}_j, \omega_j - \omega_0, \boldsymbol{y}_j) \\ \mathbf{0} &= \boldsymbol{g}_j(\boldsymbol{x}_j, \omega_j - \omega_0, \boldsymbol{y}_j)\ . \end{aligned} \tag{1}$$

The work of F. Bizzarri was partially supported by Italian MUR under the grant PRIN 2022 DCNanoSyn, CUP D53D23001500006, project code 2022SPFP9R. Funded by EU – Next Generation EU.

[1]In this work, as done in [9], we model GFM CIGs by resorting to the swing equation. Hence, the extension to the case in which GFM CIGs are present is straightforward. The presence of GFL CIGs is also considered in our case study in Sec. IV but, for the sake of simplicity, GFL CIGs are not considered in presenting the generic mathematical model of the system since it would be much more involved and it would provide a limited added value.

The meaning of the symbols in (1) for the $j-$th SG is as follows:

- Ω: the base synchronous frequency in $\mathrm{rad/s}$;
- $\omega_j(t)$: the per-unit (pu) rotor speed;
- $\omega_0 \in \mathbb{R}$: the pu reference synchronous frequency;
- $\delta_j(t)$: the rotor angle;
- $\mathcal{M}_j$: twice the product of the inertia constant H_j and the pu rated power S_{B_j}, $\mathcal{M}_j = 2H_jS_{B_j}$;
- $\mathcal{D}_j$: the product of the load damping factor D_j and the pu rated power S_{B_j}, $\mathcal{D}_j = D_jS_{B_j}$;
- $P_{e_j}(\cdot)$: the SG pu electrical active power exchange;
- $P_{m_j}(\cdot)$: the SG pu mechanical power of the machines, regulated by their respective turbine governors;
- $\boldsymbol{f}_j : \mathbb{R}^{n_j+m_j+1} \to \mathbb{R}^{n_j}$ and $\boldsymbol{g}_j : \mathbb{R}^{n_j+m_j+1} \to \mathbb{R}^{m_j}$: the vector field and the algebraic constraints, respectively, of the DAEs of the turbine governor of the $j-$th generator;
- $\boldsymbol{x}_j \in \mathbb{R}^{n_j}$ and $\boldsymbol{y}_j \in \mathbb{R}^{m_j}$: the state and algebraic variables, respectively, of the turbine governor of the $j-$th SG.

The classical model in (1) represents the envelope of the actual power system dynamics through a steady-state solution. Indeed, the periodic steady-state solution at the fundamental frequency with a constant envelope is represented as a constant steady-state solution, i.e., a stationary solution in the dq-frame. Therefore, a stationary solution of (1) is not an isolated equilibrium but rather is embedded in a continuum of equilibria [10]. This is confirmed by the presence of a null eigenvalue in the Jacobian matrix of the power system model linearized around an equilibrium point [11].

A generic power system can be viewed as a power-controlled oscillator whose instantaneous frequency (i.e., rotor speed of synchronous generators) is controlled by the power flows. In reality, the power system model is more complex than this since it includes several power-controlled oscillators (viz., synchronous generators and GFM CIGs) [8], [12]. In any case, no matter how complex a power system, two aspects always hold true: (i) the frequency of its generators (oscillators) deviate whenever power generation and demand do not match; (ii) interconnected generators share the same instantaneous oscillation frequency when synchronized.

It is common knowledge that power system generators achieve synchronization in the low-frequency range [8]. This implies that, although the rotating speed of each generator may evolve differently right after a power mismatch, they become the same in the low-frequency range (and at steady-state)[2].

This last concept is at the core of our method. Before explaining it, however, we first introduce the small-signal power system model and the *principal frequency system dynamics*.

B. The small-signal model

In the following, $\mathbb{1}_k$ is the $k \times k$ identity matrix and $\mathbb{1}_{k,h}$ is a $k \times h$ matrix of ones. We introduce the vectors $\boldsymbol{\delta}$, $\boldsymbol{\omega}$, $\boldsymbol{x}$, $\boldsymbol{y}$, $\boldsymbol{P_m}$, and $\boldsymbol{P_e}$ as the stacked versions of the corresponding scalar quantities. In particular, being $n = n_1 + \cdots + n_N$ and $m = m_1 + \cdots + m_N$, $\boldsymbol{x} \in \mathbb{R}^n$ and $\boldsymbol{y} \in \mathbb{R}^m$. In the same way, $\boldsymbol{f} : \mathbb{R}^{n+m+N} \to \mathbb{R}^n$ and $\boldsymbol{g} : \mathbb{R}^{n+m+N} \to \mathbb{R}^m$ are the stacked versions of the $\boldsymbol{f}_j$ and $\boldsymbol{g}_j$ vector functions. $\boldsymbol{\mathcal{M}} \in \mathbb{R}^{N\times N}$ and $\boldsymbol{\mathcal{D}} \in \mathbb{R}^{N\times N}$ are diagonal matrices whose j-th elements are $\mathcal{M}_j$ and $\mathcal{D}_j$, respectively.

Starting from the model of a single SG in (1), the small-signal model of the entire power system can be written as

$$\begin{aligned} \Delta\dot{\boldsymbol{\delta}} &= \Omega\Delta\boldsymbol{\omega} \\ \boldsymbol{\mathcal{M}}\Delta\dot{\boldsymbol{\omega}} &= \boldsymbol{J_1}\Delta\boldsymbol{x} - \boldsymbol{P_{e_\delta}}\Delta\boldsymbol{\delta} + (\boldsymbol{J_2} - \boldsymbol{\mathcal{D}})\,\Delta\boldsymbol{\omega} + \boldsymbol{\Gamma u}(t) \\ \Delta\dot{\boldsymbol{x}} &= \boldsymbol{J_3}\Delta\boldsymbol{x} + \boldsymbol{J_4}\Delta\boldsymbol{\omega}\ , \end{aligned}$$

where $\boldsymbol{u}(t) \in \mathbb{R}^U$ is a small signal emulating the injection of (stochastic) disturbances or probing signals in U buses of the power system, $\boldsymbol{\Gamma} \in \mathbb{R}^{N\times U}$ models how $\boldsymbol{u}(t)$ affects the dynamics of each rotor speed, $\boldsymbol{J_1} = \boldsymbol{P_{m_x}} - \boldsymbol{P_{m_y}}\boldsymbol{g_y}^{-1}\boldsymbol{g_x}$, $\boldsymbol{J_2} = \boldsymbol{P_{m_\omega}} - \boldsymbol{P_{m_y}}\boldsymbol{g_y}^{-1}\boldsymbol{g_\omega}$, $\boldsymbol{J_3} = \boldsymbol{f_x} - \boldsymbol{f_y}\boldsymbol{g_y}^{-1}\boldsymbol{g_x}$, $\boldsymbol{J_4} = \boldsymbol{f_\omega} - \boldsymbol{f_y}\boldsymbol{g_y}^{-1}\boldsymbol{g_\omega}$, and $\boldsymbol{P_{e_\delta}} \in \mathbb{R}^{N\times N}$ is the network interconnection Laplacian *singular* matrix [13], whose null space is spanned by $\mathbb{1}_{N,1}$[3]. We now introduce the principal frequency system dynamics, which correspond to the frequency of the center of inertia (COI) [14]

$$\omega_{\mathrm{COI}}(t) = \frac{\sum_{j=1}^{N} S_{B_j}H_j\omega_j(t)}{\sum_{j=1}^{N} S_{B_j}H_j}\ .$$

As previously stated, the rotor speed deviation of each generator at low frequency is the same and equal to $\Delta\omega_1 = \Delta\omega_2 = ... = \Delta\omega_N = \Delta\omega_{\mathrm{COI}}(t)$. As a result, the instantaneous rate of change of frequency of the COI can be derived as

$$\Delta\dot{\omega}_{\mathrm{COI}}(t) = \mathcal{G}_M^{-1}\ \mathbb{1}_{1,N}\boldsymbol{\mathcal{M}}\Delta\dot{\boldsymbol{\omega}}|_{\Delta\boldsymbol{\omega}=\mathbb{1}_{N,1}\Delta\omega_{\mathrm{COI}}(t)}$$

that in the Laplace's domain reads as

$$\Delta\omega_{\mathrm{COI}}(s) = \frac{\upsilon(s)}{\mathcal{G}_M s + \mathbb{1}_{1,N}\boldsymbol{\Upsilon}(s)\mathbb{1}_{N,1} + \mathcal{G}_D}\ ,$$

where $\upsilon(s) = \mathbb{1}_{1,N}\boldsymbol{\Gamma u}(s)$, $\mathcal{G}_M = \mathbb{1}_{1,N}\boldsymbol{\mathcal{M}}\mathbb{1}_{N,1}$ is the *global inertia* of the power system , $\mathcal{G}_D = \mathbb{1}_{1,N}(\boldsymbol{\mathcal{D}} - \boldsymbol{J_2})\mathbb{1}_{N,1}$ is the *global damping*, and $\boldsymbol{\Upsilon}(s) = \boldsymbol{J_1}\left(\boldsymbol{J_3} - s\mathbb{1}_N\right)^{-1}\boldsymbol{J_4}$. Since $\boldsymbol{J_1}$, $\boldsymbol{J_3}$, and $\boldsymbol{J_4}$ are block-diagonal matrices made up of N blocks of size $1 \times n_j$, $n_j \times n_j$, and $n_j \times 1$ (for $j = 1, \ldots, N$), respectively, the $\boldsymbol{\Upsilon}(s)$ matrix is simply diagonal: each element $\Upsilon_{jj}(s)$ is a rational function with n_j poles[4], such that

$$\mathbb{1}_{1,N}\boldsymbol{\Upsilon}(s)\mathbb{1}_{N,1} = \sum_{j=1}^{N}\frac{b_j(s)}{s^{n_j} + a_{(n_j-1)_j}s^{n_j-1} + \cdots + a_{(0)_j}}\ ,$$

[2]Generator synchronization is never observed in practice but *on average* due to random fluctuations in load consumption and RES generation, which continuously stimulate the generators and prevent reaching steady-state operation.

[3]Some variables are not described for brevity but have similar meaning. For instance, $\boldsymbol{f_x}$ is the Jacobian matrix of the vector function $\boldsymbol{f}$ w.r.t. $\boldsymbol{x}$.

[4]It is worth noticing that, being $\boldsymbol{B}$ a generic $Q \times P$ matrix, $\mathbb{1}_{1,Q}\boldsymbol{B}\mathbb{1}_{P,1}$ yields the summation of all the entries of $\boldsymbol{B}$.

where $\deg(b_j(s)) < n_j$. Hence,

$$\Delta\omega_{\text{COI}}(s) = \frac{\upsilon(s)}{\mathcal{G}_M s + \mathcal{G}_D + \frac{P_1(s)}{s^L + \tilde{a}_{L-1}s^{L-1} + \cdots + \tilde{a}_0}} = \underbrace{\frac{\upsilon(s)}{\mathcal{G}_M}}_{\nu(s)} \frac{s^L + \tilde{a}_{L-1}s^{L-1} + \cdots + \tilde{a}_0}{s^{L+1} + \underbrace{\left(\tilde{a}_{L-1} + \frac{\mathcal{G}_D}{\mathcal{G}_M}\right)}_{\mu} s^L + P_2(s)}, \quad (2)$$

where $L \leq n$, $P_1(s)$ and $P_2(s)$ are polynomials of the variable s with $\deg(P_1(s)) < L$, and $\deg(P_2(s)) < L$. Equation (2) suggests that power system global inertia and damping can be estimated through the $\nu(s)$ and μ terms, respectively. How this can be done is described in the next section.

III. The Proposed Estimation Method

Equation (2) provides the expression of the frequency spectrum almost shared by all the $\Delta\omega_j(t)$ rotor speeds (as well as the virtual rotor speeds of possibly connected GFMs providing virtual inertia) at low frequency under the assumption of synchronization. The proposed method exploits the overlap in the frequency spectra to estimate $\mathcal{G}_M$ and $\mathcal{G}_D$ as follows:

- Assume that at least one of the generators in (1) is a GFM CIG providing a virtual inertia constant $M_{\bar{k}}$ (with $\bar{k} \in [1, \ldots, N]$). By acting on the CIG converter controls, we modulate $M_{\bar{k}}$ by letting it vary as a square waveform of amplitude $\Delta\mathcal{M}$, period $T_{\Delta\mathcal{M}}$, and duty cycle 50%.
- We simultaneously modulate the power injected at a generic power system bus by a discrete set of $\mathcal{N}_\mathcal{T}$ deterministic and coherent small-signal sinusoidal tones $s_w(t)$ ($w = 1, \ldots, \mathcal{N}_\mathcal{T}$). Since only the low frequency portion of the $\omega_{\text{COI}}(s)$ spectrum is of interest, the $s_w(t)$ waveforms are very slowly varying; they are also of modest magnitude to avoid impacting the stability of the power system [15]. Their only purpose is to continuously stimulate the grid and allow measuring the change in one of the N rotor speeds, say $\omega_{\bar{j}}$ with $\bar{j} \in [1, \ldots, N]$. The optimal selection of $\mathcal{N}_\mathcal{T}$ and of the f_w frequency of each tone depends on the bandwidth that has to be explored to fit (2).
- We compute the γ_{w_c} and γ_{w_s} direct and quadrature components of the Fourier integrals of $\omega_{\bar{j}}$ at each f_w frequency as

$$\gamma_{w_c} + i\gamma_{w_s} = \frac{f_w}{\kappa} \int_{t_0}^{t_0 + \frac{\kappa}{f_w}} \omega_{\bar{j}}(t) e^{i2\pi f_w t} dt \ , \quad (3)$$

  where i is the imaginary unit ($i^2 = -1$), $\kappa \in \mathbb{N}^+$, and γ_{w_c} and γ_{w_s} are the frequency samples of $\Delta\omega_{\text{COI}}(s)$.
- The vector fitting (VF) algorithm [16]–[18] is applied on $\Delta\omega_{\text{COI}}(s)$ with the specific purpose of deriving $\mathcal{G}_M$ and $\mathcal{G}_D$. In particular, we fit the frequency spectrum of $\omega_{\bar{j}}(t)$ before and after varying $\mathcal{M}_{\bar{k}}$, thus obtaining $\nu_- = \upsilon/\mathcal{G}_M$, $\nu_+ = \upsilon/(\mathcal{G}_M + \Delta\mathcal{M})$, $\mu_- = \tilde{a}_{L-1} + \mathcal{G}_D/\mathcal{G}_M$, and $\mu_+ = \tilde{a}_{L-1} + \mathcal{G}_D/(\mathcal{G}_M + \Delta\mathcal{M})$. These parameters allow us to derive

$$\mathcal{G}_M = \frac{\nu_+}{\nu_- - \nu_+}\Delta\mathcal{M}, \ \mathcal{G}_D = \nu_-\nu_+\frac{\mu_- - \mu_+}{(\nu_- - \nu_+)^2}\Delta\mathcal{M} \ . \quad (4)$$

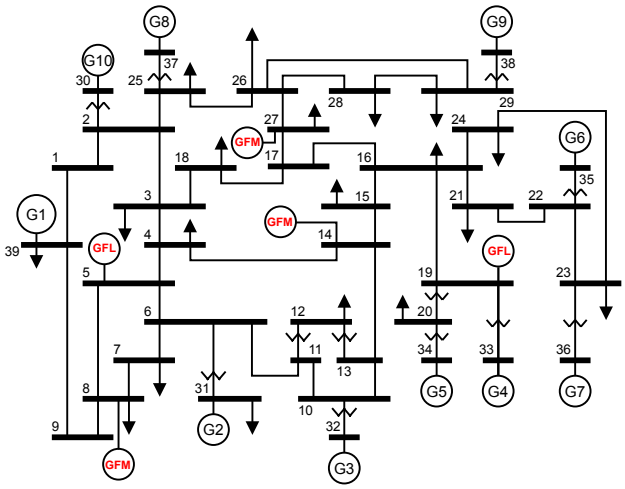

Fig. 1. Schematic of the modified IEEE 39-BUS system. The $j-$th SG is equipped with a turbine governor described by the ODE $T_a\dot{x}_j = -k_a(\omega_j - \omega_0) - (x_j - \bar{P}_{m_j})$, $P_{m_j}(x_j, \omega_j - \omega_0) = x_j$, and $\bar{P}_{m_j}$ is its mechanical-power setpoint corresponding to the power flow solution.

The proposed method requires no information about the network except the $\omega_{\bar{j}}(s)$ frequency spectrum that can be computed from the controller of a GFM CIG. The modulation of $\mathcal{M}_{\bar{k}}$ is necessary since the value of $\upsilon(s)$, even if it is constant when injecting a purely sinusoidal probing tone, is unknown as the $\mathbf{\Gamma}$ matrix is unknown too and so is how it redistributes in the power system and affects rotor speeds.

In practice, it is not possible to periodically modulate the inertia constant of the SGs nor to sample the time evolution of their rotor speed. For this reason, we exploit a GFM CIG that is either already present in the grid, or can be inserted with the specific purpose of allowing the estimation of the power system global inertia and damping. Moreover, also the probing signals used to stimulate the power system in a suitable frequency band are injected by the GFM CIG. As such, the requirements for applying this method can easily be met[5].

IV. A Case Study

We tested the proposed algorithm on a modified version of the IEEE 39-BUS system [19], whose schematic is reported in Fig. 1[6]. The original grid, which corresponds to a simplified model of the New England power system, contains 10 generators (see Table I) and 46 lines. We modified the system by adding three GFM CIGs characterized by a 50 s inertia constant and a 100 MVA rated apparent power. They are connected at BUS8, BUS14 and BUS27, with the generated power set at, respectively 1 pu, 0.5 pu, and 0.25 pu[7]. In addition, two

[5]If the effects of noise must be reduced to increase the signal-to-noise ratio, the integrals in (3) can be computed over a time interval μ/f_w which is a multiple of the period of the corresponding tone $s_w(t)$. The t_0 time instant in (3) coincides with the rising and falling edges of the square waveform used to periodically change the $\mathcal{M}_{\bar{k}}$ virtual inertia. Assuming $s_1(t)$ as the tone with the lowest frequency, f_1 suggests how to choose $T_{\Delta\mathcal{M}}$, i.e., $T_{\Delta\mathcal{M}}/2 > \mu/f_1$.

[6]The IEEE 39-BUS system version we started from is that supplied with DIgSILENT PowerFactory.

[7]Due to space reasons, it is not possible to write here the DAEs governing GFM and GFL CIGs. The interested reader can find them in [9].

TABLE I
SYNCHRONOUS GENERATORS H AND S_B ($S_{\text{BASE}} = 100\,\text{MVA}$).

Gen.	H [s]	S_B [pu]	Gen.	H [s]	S_B [pu]
G_1	5.00	100	G_6	4.35	8
G_2	4.33	7	G_7	3.77	7
G_3	4.47	8	G_8	3.47	7
G_4	3.57	8	G_9	3.45	10
G_5	4.33	6	G_{10}	4.20	10

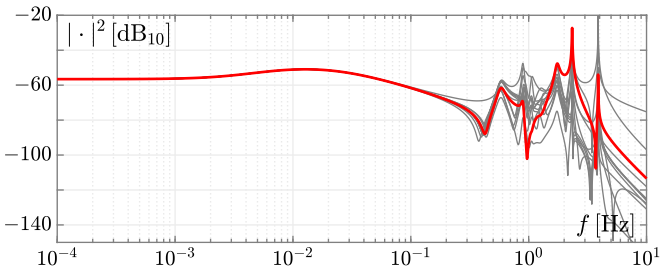

Fig. 2. The magnitude squared of the transfer functions between the small-signal input implemented by the GFM CIG at BUS14 and the rotor speed of each synchronous generator and GFM providing virtual inertia.

GFL CIGs are connected at BUS19 and BUS5, respectively, (rated apparent power 100 MVA, generated power 0.01 pu, and virtual damping set at 10 pu and 5 pu, respectively). The GFM CIG used to modulate $\mathcal{G}_M$, to inject the probing signals and to sample its virtual rotor speed, as described in Sec. III, is the one connected at BUS14.

To show how the $\omega_{\text{COI}}(s)$ spectrum builds up, we firstly performed an (ideal) frequency scan injecting small-signal sinusoidal tones through the CIG at BUS14 in a noiseless setup (no stochastic variations of the loads). By doing so, we computed all the transfer functions between the small-signal input and the rotor speed of each synchronous machine and CIG (see Figure 2). We can notice that they almost perfectly overlap at frequencies below 0.1 Hz while they sensibly differ for higher frequency values. Note that these transfer functions show how rotor speeds deviate from ω_0 under the assumption of small-signal behavior (linear behavior in the neighborhood of an equilibrium point). By observing the low frequency overlap of all the curves in Fig. 2, the global inertia and damping can be determined through (4) by fitting *only* the low frequency portion of the spectrum related to the CIG connected at BUS14. We selected the $[6, 30]$ mHz frequency interval, since all (virtual) rotor speeds are described by the same behavior in this frequency interval (principal frequency system dynamics), as predicted by our analysis.

To work in a more realistic framework, we followed the steps described in Sec. III. We used independent zero-mean small-signal stochastic noise sources, one for each power load of the IEEE 39-BUS system, thus emulating stochastic fluctuations by means of a multi-dimensional Ornstein-Uhlenbeck (OU) process [20] $\boldsymbol{\eta}(t)$ as was done in [21]. The spectra of OU processes are an accurate model of those due to the stochastic variability of power loads [22]–[25]. The zero mean implies that on average the loads power fluctuations do not perturb the operating point of the system. We chose $0.5\,\text{s}^{-1}$ as the

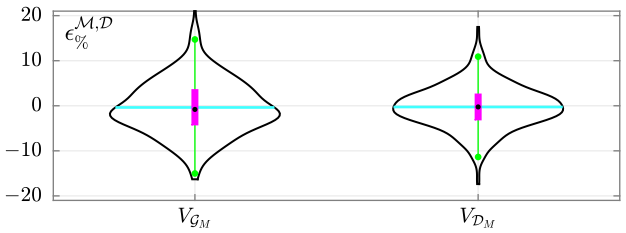

Fig. 3. The $\epsilon_{\%}^{\mathcal{M}} = 100(\mathcal{G}_M - \mathcal{G}_M^{\text{act}})/\mathcal{G}_M^{\text{act}}$ and $\epsilon_{\%}^{\mathcal{D}} = 100(\mathcal{G}_D - \mathcal{G}_D^{\text{act}})/\mathcal{G}_D^{\text{act}}$ percent relative errors. The horizontal cyan segments and the black solid circle markers correspond to the mean μ and the median μ_{dn} of the results, respectively. The magenta bars represent the IQR, viz. the spread difference between the 75^{th} and 25^{th} percentiles of the data. The green solid circle markers represent the upper adjacent value (i.e., the largest observation that is less than or equal to the third quartile plus $1.5\times$IQR) and the lower adjacent value (i.e., the smallest observation that is greater than or equal to the first quartile minus $1.5\times$IQR). The $V_{\mathcal{G}_M}$ violin plot ($\mu = -0.379$, $\mu_{\text{dn}} = -0.810$, and IQR $= 7.746$) and the $V_{\mathcal{G}_D}$ violin plot ($\mu = -0.274$, $\mu_{\text{dn}} = -0.257$, and IQR $= 5.657$) refer to the global momentum and global load damping estimation, respectively, obtained by injecting a set of $\mathcal{N}_{\mathcal{T}} = 10$ deterministic and coherent small signal sinusoidal tones through the GFM CIG connected at BUS14.

mean-reversion speed of $\boldsymbol{\eta}(t)$ and its variance in such a way that the standard deviation of the fluctuation of each load is 0.5% of its nominal active power. To carry out time-domain simulations, the numerical integration of $\boldsymbol{\eta}(t)$ was based on the numerical scheme proposed by Gillespie [26]. We used the second-order trapezoidal implicit weak scheme for stochastic differential equations with colored noise [27], available in the simulator PAN [28]–[30].

Instead of performing a frequency scan, we used the CIG connected to BUS14 to inject a discrete set of $\mathcal{N}_{\mathcal{T}} = 10$ deterministic and coherent small-signal sinusoidal tones, whose magnitude caused a peak power variation smaller than 2.5% of the nominal power of the IEEE 39-BUS system. Then, we performed 500, each 15 min-long, large-signal time domain simulations. For each run, we used the VF method to fit the frequency behavior of the virtual rotor speed of the CIG connected to BUS14 before and after changing its virtual inertia constant, and estimated the $\mathcal{G}_M$ global inertia and the $\mathcal{G}_D$ global damping. The left and right violin plots in Fig. 3 summarize the performance of the proposed approach, in terms of the percent relative error, in estimating $\mathcal{G}_M$ and $\mathcal{G}_D$ for each of the 500 random configurations w.r.t. its actual value $\mathcal{G}_M^{\text{act}}$ and $\mathcal{G}_D^{\text{act}}$, respectively. The accuracy of the estimates is proven by the mean, median, and IQR values reported in the figure caption.

V. CONCLUDING REMARKS

Contrary to the majority of the methods presented in the literature, the proposed method estimates the inertia and damping values of the entire power system and not of a single synchronous or virtual generator. Moreover, the low relative errors and the estimation time of 15 min make it an adequate candidate for real time applications. Another key feature of this method is its practical applicability. Indeed, it allows estimating inertia and damping of power system in noisy operating conditions and comprising converter-interfaced elements just by exploiting a single GFM CIG.

REFERENCES

[1] P. Denholm, T. Mai, R. Kenyon, B. Kroposki, and M. O'Malley, "Inertia and the power grid: A guide without the spin," Golden, CO: National Renewable Energy Laboratory, Tech. Rep. NREL/TP-6120-73856, 2020.

[2] E. O. Kontis, I. D. Pasiopoulou, D. A. Kirykos, T. A. Papadopoulos, and G. K. Papagiannis, "Estimation of power system inertia: A comparative assessment of measurement-based techniques," *Electr. Pow. Syst. Res.*, vol. 196, p. 107250, 2021.

[3] S. C. Dimoulias, E. O. Kontis, and G. K. Papagiannis, "Inertia Estimation of Synchronous Devices: Review of Available Techniques and Comparative Assessment of Conventional Measurement-Based Approaches," *Energies*, vol. 15, no. 20, pp. 1–30, 2022.

[4] K. Prabhakar, S. K. Jain, and P. K. Padhy, "Inertia estimation in modern power system: A comprehensive review," *Electr. Pow. Syst. Res.*, vol. 211, p. 108222, 2022.

[5] J. W. Pierre, N. Zhou, F. K. Tuffner, J. F. Hauer, D. J. Trudnowski, and W. A. Mittelstadt, "Probing signal design for power system identification," *IEEE Trans. Power Syst.*, vol. 25, no. 2, pp. 835–843, 2010.

[6] N. Zhou, J. Pierre, and J. Hauer, "Initial results in power system identification from injected probing signals using a subspace method," *IEEE Trans. Power Syst.*, vol. 21, no. 3, pp. 1296–1302, 2006.

[7] R. Chakraborty, H. Jain, and G. S. Seo, "A review of active probing-based system identification techniques with applications in power systems," *International Journal of Electric Power and Energy Systems*, vol. 140, p. 108008, 2022.

[8] A. Sajadi, R. W. Kenyon, and B. M. Hodge, "Synchronization in electric power networks with inherent heterogeneity up to 100% inverter-based renewable generation," *Nature Communications*, vol. 13, no. 1, 2022.

[9] B. Barać, M. Krpan, T. Capuder, and I. Kuzle, "Modeling and initialization of a virtual synchronous machine for power system fundamental frequency simulations," *IEEE Access*, vol. 9, pp. 160 116–160 134, 2021.

[10] B. Aulbach, *Continuous and Discrete Dynamics Near Manifolds of Equilibria*, ser. Lecture Notes in Mathematics. Springer-Verlag, 1984.

[11] P. Sauer and M. A. Pai, "Power system steady-state stability and the load-flow jacobian," *IEEE Trans. Power Syst.*, vol. 5, no. 4, pp. 1374–1383, Nov. 1990.

[12] A. E. Motter, S. A. Myers, M. Anghel, and T. Nishikawa, "Spontaneous synchrony in power-grid networks," *Nature Physics*, vol. 9, no. 3, p. 191 – 197, 2013.

[13] J. Machowski, Z. Lubosny, J. Bialek, and J. Bumby, *Power System Dynamics: Stability and Control*. Wiley, 2020.

[14] P. Kundur, N. Balu, and M. Lauby, *Power system stability and control*, ser. EPRI power system engineering series. McGraw-Hill, 1994.

[15] R. Pintelon and J. Schoukens, *Design of Excitation Signals*, 2012, pp. 151–175.

[16] B. Gustavsen and A. Semlyen, "Rational approximation of frequency domain responses by vector fitting," *IEEE Trans. Power Del.*, vol. 14, no. 3, pp. 1052–1061, 1999.

[17] B. Gustavsen, "Improving the pole relocating properties of vector fitting," *IEEE Trans. Power Del.*, vol. 21, no. 3, pp. 1587–1592, 2006.

[18] P. Triverio, *Vector Fitting, in Handbook on Model Order Reduction*. De Gruyter, Berlin, 2021.

[19] T. Athay, R. Podmore, and S. Virmani, "A Practical Method for the Direct Analysis of Transient Stability," *IEEE Trans. Power App. Syst.*, vol. PAS-98, no. 2, pp. 573–584, Mar./Apr. 1979.

[20] L. Arnold, *Stochastic differential equations*, ser. A Wiley-Interscience publication. Wiley, 1974.

[21] F. Bizzarri, D. del Giudice, S. Grillo, D. Linaro, A. Brambilla, and F. Milano, "Inertia estimation through covariance matrix," *IEEE Trans. Power Syst.*, vol. 39, no. 1, pp. 947–956, 2024.

[22] R. H. Hirpara and S. N. Sharma, "An Ornstein-Uhlenbeck process-driven power system dynamics," *IFAC-PapersOnLine*, vol. 48, no. 30, pp. 409–414, 2015, 9th IFAC Symposium on Control of Power and Energy Systems CPES 2015.

[23] C. Nwankpa and S. Shahidehpour, "Colored noise modelling in the reliability evaluation of electric power systems," *Appl. Math. Model.*, vol. 14, no. 7, pp. 338–351, 1990.

[24] F. Milano and R. Zárate-Miñano, "A systematic method to model power systems as stochastic differential algebraic equations," *IEEE Trans. Power Syst.*, vol. 28, no. 4, pp. 4537–4544, Nov. 2013.

[25] C. Roberts, E. M. Stewart, and F. Milano, "Validation of the ornstein-uhlenbeck process for load modeling based on μPMU measurements," in *2016 Power Systems Computation Conference (PSCC)*, 2016, pp. 1–7.

[26] D. T. Gillespie, "Exact numerical simulation of the ornstein-uhlenbeck process and its integral," *Phys. Rev. E*, vol. 54, pp. 2084–2091, Aug 1996.

[27] G. N. Milshtein and M. V. Tret'yakov, "Numerical solution of differential equations with colored noise," *Journal of Statistical Physics*, vol. 77, no. 3, pp. 691–715, 1994.

[28] F. Bizzarri and A. Brambilla, "PAN and MPanSuite: Simulation vehicles towards the analysis and design of heterogeneous mixed electrical systems," in *NGCAS, Genova, Italy*, Sept. 2017, pp. 1–4.

[29] F. Bizzarri, A. Brambilla, G. Storti Gajani, and S. Banerjee, "Simulation of real world circuits: Extending conventional analysis methods to circuits described by heterogeneous languages," *IEEE Circuits Syst. Mag.*, vol. 14, no. 4, pp. 51–70, 2014.

[30] D. Linaro, D. del Giudice, F. Bizzarri, and A. Brambilla, "Pansuite: A free simulation environment for the analysis of hybrid electrical power systems," *Electr. Pow. Syst. Res.*, vol. 212, 2022.